

Automatic chemical design using a data-driven continuous representation of molecules

Rafael Gómez-Bombarelli^{1,2,*}, David Duvenaud^{3,4,*}, José Miguel Hernández-Lobato^{3,5,*}, Jorge Aguilera-Iparraguirre^{1,2}, Timothy D. Hirzel^{1,2}, Ryan P. Adams^{3,6}, and Alán Aspuru-Guzik^{1,†}

¹Department of Chemistry and Chemical Biology, Harvard University

²Now at Kyulux North America Inc.

³John A. Paulson School of Engineering and Applied Sciences, Harvard University

⁴Now at Department of Computer Science, University of Toronto

⁵Now at Department of Engineering, University of Cambridge

⁶Google, Inc.

*Equal contributions

†Corresponding author, alan@aspuru.com

October 13, 2021

Abstract

We report a method to convert discrete representations of molecules to and from a multidimensional continuous representation. This generative model allows efficient search and optimization through open-ended spaces of chemical compounds.

A deep neural network was trained on hundreds of thousands of existing chemical structures to construct two coupled functions: an encoder and a decoder. The encoder converts the discrete representation of a molecule into a real-valued continuous vector, and the decoder converts these continuous vectors back to the discrete representation from this latent space.

Continuous representations allow us to automatically generate novel chemical structures by performing simple operations in the latent space, such as decoding random vectors, perturbing known chemical structures, or interpolating between molecules.

Continuous representations also allow the use of powerful gradient-based optimization to efficiently guide the search for optimized functional compounds. We demonstrate our method in the design of drug-like molecules as well as organic light-emitting diodes.

The goal of drug and material design is to propose novel molecules that have certain desirable properties. However, optimization in molecular space is extremely challenging, because the search space is large, discrete, and unstructured. Making and testing new compounds is costly and time consuming, and the number of potential candidates is overwhelming. Only about 10^8 substances have ever been synthesized, [1] whereas the range of potential drug-like molecules is estimated to be between 10^{23} and 10^{60} . [2]

Virtual screening can be used to speed up this search. [3–6] Virtual libraries containing thousands to hundreds of millions of candidates can be assayed with simulations or predictions, and only the most promising leads are selected and tested experimentally.

However, even when accurate simulations are available, [7] computational molecular design is limited by the search strategy used to explore chemical space. Current methods either exhaustively search through a fixed library, [8, 9] or use discrete local search methods such as genetic algorithms [10–15] or similar discrete interpolation techniques. [16] Although these techniques have led to useful new molecules, both approaches still face large challenges. Fixed libraries are monolithic, costly to explore fully and require hand-crafted rules to avoid impractical chemistries. The genetic generation of compounds requires the manual specification of heuristics for mutation and crossover rules. Discrete optimization methods have difficulty effectively searching large areas of chemical space because geometric cues such as gradients are not available to guide the search.

The choice of representation of molecules is at the heart of the virtual discovery challenge. Molecular representations are either graph-based, using undirected graphs with atoms as nodes and bonds as edges, or as three-dimensional arrangements of atoms. For cheminformatic purposes, these graph representations are usually converted to vector representations. Ideally, these vectors are invariant to the rotation, translation and atom indexing of the molecule. Representations derived from these graphs include chemical fingerprints, [17] convolutional neural networks on graphs [18] and similar graph-convolutions, [19] or the bag-of-bonds [20] approach. Coulomb matrices, [21] scattering transforms [22], atomic distances [23], etc. are based on 3D geometries, usually obtained at an affordable level of theory. However, none of these representations can be efficiently driven in reverse to decode molecules from optimal vectors.

A differentiable, reversible, and data-driven representation has several advantages over existing systems. First, hand-specified mutation rules are unnecessary, as new compounds can be generated automatically by modifying the vector representation and then decoding. Second, a data-driven representation can leverage large sets of unlabeled chemical compounds to automatically build an even larger implicit library, and then use the smaller set of labeled examples to build a regression model from the continuous representation to the desired properties. This lets us take advantage of large chemical databases containing millions of molecules, even when many properties are unknown for most compounds. Third, a differentiable representation allows the use of gradient-based optimization to leverage geometric information and make larger jumps in chemical space. Gradient-based optimization can be combined with Bayesian optimization methods to select compounds that are likely to be informative about the global optimum. These methods can be integrated into a closed loop that proposes new compounds, tests their properties, and uses this new information to suggest even better compounds.

Recent advances in machine learning have resulted in powerful probabilistic generative

models that, after being trained on real examples, are able to produce realistic synthetic samples. Such models usually also produce low-dimensional continuous representations of the data being modeled, allowing interpolation or analogical reasoning for natural images [24], text [25], speech, and music [26]. We apply such generative models to chemical design.

In this work, we propose the use of continuous optimization to produce novel compounds by building a learned vector-valued representation of molecules. We transform between discrete and continuous representations using a pair of neural networks trained together as an autoencoder. We apply this technique in the space of drug-like molecules and organic light-emitting diodes (OLED).

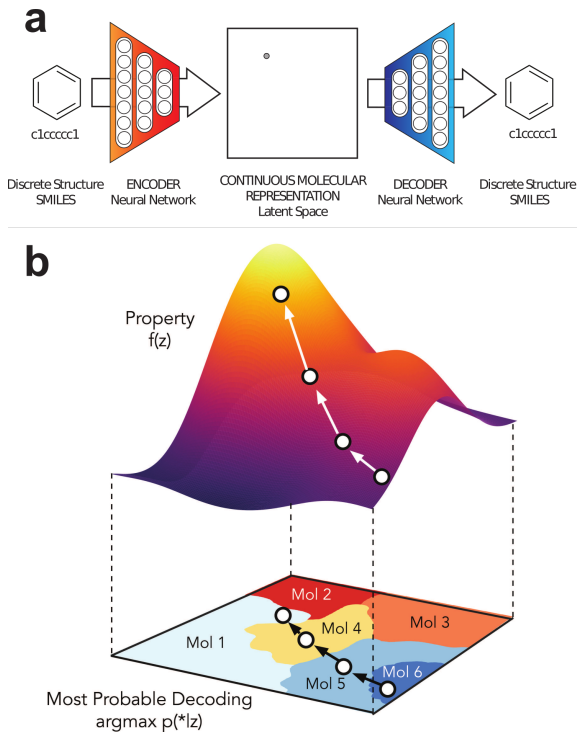


Figure 1: **a)** A diagram of the proposed autoencoder for molecular design. Starting from a discrete molecular representation, such as a SMILES string, the encoder network converts each molecule into a vector in the latent space, which is effectively a continuous molecular representation. Given a point in the latent space, the decoder network produces a corresponding SMILES string. **b)** Gradient-based optimization in continuous latent space. After training a surrogate model $f(z)$ to predict the properties of molecules based on their latent representation z , we can optimize $f(z)$ with respect to z to find new latent representations expected to have high values of desired properties. These new latent representations can then be decoded into SMILES strings, at which point their properties can be tested empirically.

Results

Initial representation of molecules Before building an encoder to a continuous representation, we must choose which discrete molecule representation to use before encoding and after decoding. To leverage the power of recent advances in sequence-to-sequence autoencoders for modeling text [25], we used the SMILES [27] representation, a commonly-used text encoding for organic molecules. We also tested InChI [28] as an alternative string representation, but found it to perform substantially worse than SMILES, presumably due to a more complex syntax that includes counting and arithmetic.

Training an autoencoder Starting from a large library of string-based representations of molecules, we trained a pair of complementary recurrent neural networks: an encoder network to convert each string into a fixed-dimensional vector, and a decoder network to convert vectors back into strings (Figure 1a). Such encoder-decoder pairs are known as *autoencoders*. The autoencoder is trained to minimize error in reproducing the original string, *i.e.*, it attempts to learn the identity function. Key to the design of the autoencoder is mapping through an *information bottleneck*. This bottleneck — here the fixed-length continuous vector — induces the network to learn a compressed representation that captures the most statistically salient information in the data. We call the vector-encoded molecule the *latent representation* of the molecule.

The character-by-character nature of the SMILES representation and the fragility of its internal syntax (opening and closing cycles and branches, allowed valences, etc.) can result in the output of invalid molecules from the decoder. Multiple factors contribute to the proportion of valid SMILES output from the decoder, including atom count and training set density. The percentage of valid SMILES output ranged from 70% to less than 1%. We employed the open source cheminformatics suite RDKit [29] and Marvin to validate the chemical structures of output molecules and discard invalid ones.

To enable molecular design, the chemical structures encoded in the continuous representation of the autoencoder need to be correlated with the target properties that we are seeking to optimize. Therefore, after training the autoencoder, we trained a third model to predict molecular properties from the latent representation. To propose promising new candidate molecules, we can start from the latent vector of an encoded molecule and then move in the direction most likely to improve the desired attribute. The resulting new candidate vectors can then be decoded into corresponding molecules. (Figure 1b)

Using variational autoencoders to produce a compact representation. For unconstrained optimization in the latent space to work, points in the latent space must decode into valid SMILES strings. However, the original training objective of the autoencoder does not enforce this constraint, potentially leading to large “dead areas” in the latent space, which decode to invalid or nonsensical SMILES strings.

To ensure that points in the latent space correspond to valid molecules, we modified our autoencoder and its objective into a *variational* autoencoder (VAE) [30]. VAEs were developed as a principled approximate-inference method for latent-variable models, in which each datapoint has a corresponding, but unknown, latent representation. VAEs generalize autoencoders, adding stochasticity to the encoder, and adding a penalty term encouraging all

areas of the latent space to correspond to a valid decoding. The intuition is that adding noise to the encoded molecules forces the decoder to learn how to decode a wider variety of latent points. In addition, since two different molecules can have their encodings stochastically brought close in the latent space, but still need to decode to different molecular graphs, this constraint also encourages the encodings to spread out over the entire latent space to avoid overlap. Using variational autoencoders with RNN encoder and decoder networks was first tried by Bowman *et al.* in the context of written sentences in English and we followed their approach closely. [25]

The autoencoder was trained on a dataset with approximately 250,000 drug-like commercially available molecules extracted at random from the ZINC database. [31] We also tested this approach on approximately 100,000 OLED molecules generated combinatorially. [9]

We performed Bayesian optimization over hyperparameters specifying the deep autoencoder architecture and training, such as the choice between a recurrent or convolutional encoder, the number of hidden layers, layer sizes, regularization and learning rates. [32] We also ran an outer loop of optimization to determine how small the latent dimension could be while still producing reasonable reconstruction error. After training naïve and variational autoencoders on drug-like molecules, the same structure was also used with organic-light emitting (OLED) molecules.

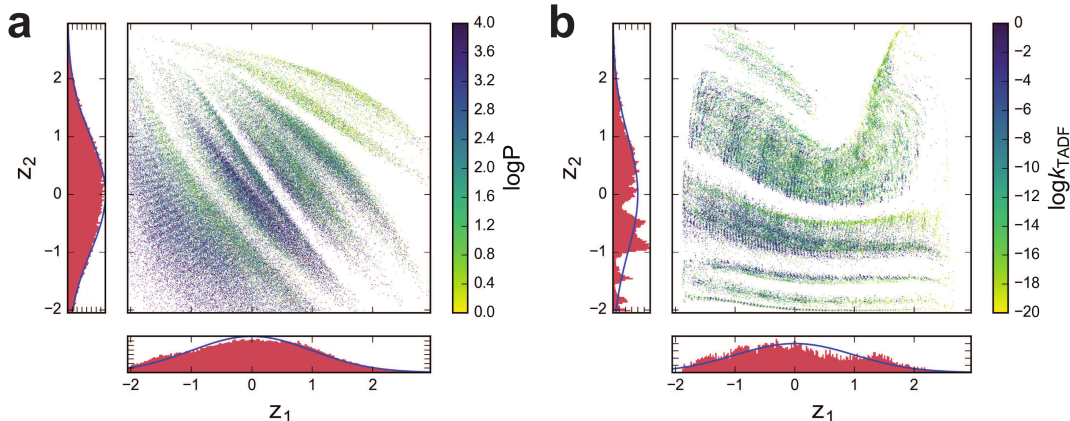


Figure 2: Projection of the molecular training sets onto learned two-dimensional latent spaces. The one-dimensional histograms show the distribution of the training data along each dimension, overlaid with the Gaussian prior imposed in the variational autoencoder. The points are colored according to a chemical property relevant to their function. *Left*: A natural library of drug-like molecules, colored by their predicted water-octanol partition coefficient. *Right*: A combinatorially-generated library of organic LED molecules, colored by their predicted delayed fluorescent emission rate (k_{TADF} in μs^{-1}).

To produce a visualization of chemical libraries, we trained autoencoders with 2-dimensional latent spaces. Figure 2 shows two separate libraries encoded into their respective latent spaces. In the case of the drug-like molecules, since they are a diverse, natural training set, we observed that the molecules are spread quite evenly across the space and they follow the Gaussian prior very closely along both dimensions. On the other hand, the distribution

of the OLED molecules could not be effectively regularized into a Gaussian shape and is more structured along each dimension. We believe this is a consequence of the combinatorial donor-bridge-acceptor generation procedure used to create the OLED library.

In both projections, even in the well-regularized drug-like set, we observe banding and structure in the 2D space at multiple scales. This showcases the ability of the deep autoencoder to address molecular similarity while mapping a discrete to a continuous representation. Interestingly, the plotted molecular properties show a marked dependency on the latent coordinates; nearby molecules tend to have similar properties. That ability to reflect structure-property relationships is a desired feature for any molecular representation. This result is particularly encouraging since these autoencoders were trained in an unsupervised way, independently of target properties.

Table 1 compares the ability of our best drug-like and OLED autoencoder to reconstruct the train and test sets both for naïve and variational configurations, confirming the greater challenge of learning a latent representation with the machine-generated OLED library.

| Molecular family | Autoencoder training loss | Latent dimensions | Training set reconstruction % | Test set reconstruction % |
|------------------|---------------------------|-------------------|-------------------------------|---------------------------|
| drug-like | naïve | 56 | 99.1 | 98.3 |
| drug-like | variational | 292 | 96.4 | 95.3 |
| OLED | naïve | 56 | 96.7 | 91.2 |
| OLED | variational | 292 | 91.4 | 79.4 |

Table 1: Reconstruction accuracy for the deep autoencoders used in this work. Accuracy is defined as the percentage of position-to-position correct characters in decoded SMILES strings where the character with highest probability is always selected. An autoencoder with a large enough number of latent dimensions could achieve perfect reconstruction, but exploration of the latent space tends to become more difficult as dimensionality increases.

Perturbation and interpolation in molecular space We analyzed the performance of the VAE in a number of tasks involving encoding and decoding molecular structures.

Figure 3a shows the result of encoding the chemical structure of aspirin by sampling the VAE and then decoding the latent representation. Multiple chemical variations of the original compounds were obtained as a consequence of both the probabilistic sampling of the VAE and stochastic nature of the SMILES string decoding. We show the set without repetition of the output molecules regardless of their relative frequencies, hence over-representing rarely-generated compounds. In addition, a set of compounds from the list of 1386 FDA approved drugs were selected at random, [33] and subject to the same stochastic encode-decode process (Figures 6 and 7).

Figures (8 and 9) show multiple decodings of eight randomly-sampled points in the latent space, akin to playing spin-the-globe in high dimensional space. The random points generally decode into mid-sized valid molecules, suggesting that the VAE is effective at ensuring that points in the latent space map to valid structures. The variation within the molecules decoded for each point in latent space is due to the stochastic nature of the decoder.

In addition to sampling points in latent space, we analyzed the meaning of directions in the latent space. Following the success of generative models of images, we performed

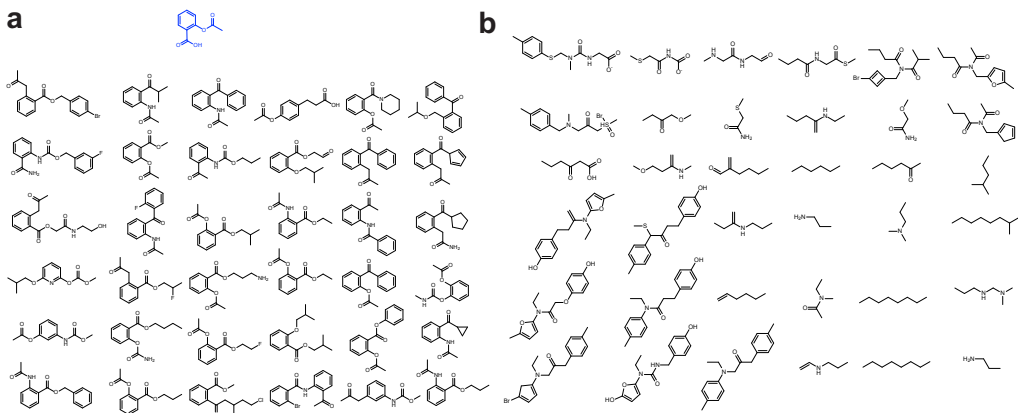


Figure 3: **a)** Random sampling. Molecules decoded from randomly-sampled points in the latent space of a variational autoencoder, near to a given molecule (aspirin [2-(acetyloxy)benzoic acid], highlighted in blue). **b)** Interpolation. Two-dimensional interpolation between four random points in in drug-like VAE. Decodings of interpolating linearly between the latent representations of the four molecules in the corners.

interpolations in chemical space. Starting points in the latent space were selected; we then performed a linear grid interpolation over two dimensions. We decoded each point in latent space multiple times and report the molecule whose latent representation, once re-encoded, is closest to the sampled point (Figures 3b and 11-10)

In a related experiment, and starting from a random FDA-approved drug molecule, two random unitary vectors in latent space were followed and decoded into molecules. Figures 13-15) show the starting molecule in the center, and the most probable decodings of the extrapolated molecules on the horizontal and vertical direction. Most points along the path through latent space decode to valid molecules.

Bayesian optimization of logP Having shown the ability of a VAE to generate a continuous, reversible encoding of molecular structures, we proceeded to test its potential to discover new molecules with desired properties.

We first attempted to maximize the water-octanol partition coefficient (logP), an important measure in drug design that characterizes the drug-likeness of a molecule. To ensure that the resulting molecules would be easy to synthesize in practice, we also incorporated the synthetic accessibility [34] (SA) score into our objective. RDkit was used to calculate logP and SA score. [35]

Our initial experiments optimizing the logP and SA scores produced novel molecules, but ones having unrealistically large rings of carbon atoms. To avoid this problem, we added a penalty for having carbon rings of size larger than 6 to our objective.

Thus our preferred objective for a given molecule m is given by:

$$J^{\log P}(m) = \log P(m) - \text{SA}(m) - \text{ring-penalty}(m), \quad (1)$$

where the scores $\log P(m)$, $\text{SA}(m)$, and $\text{ring-penalty}(m)$ are normalized to have zero mean and unit standard deviation across the training data.

More than half of the 500 latent feature vectors selected by the above process produced a valid SMILES string. Among the resulting molecules, the two best had objective values of 5.02 and 4.68, higher than the best objective value in the training data, 4.52. Figure 4b shows the empirical distribution of objective values for the molecules in the training data. The two new molecules are shown Figure 4a.

A high value of the objective eq. (1) does not necessarily translate into a high logP score. However, the logP scores for the molecules from Figure 4a are 8.07 and 8.51, while the highest logP score in the training data is 8.25. Therefore, the second molecule has higher logP score than any molecule in the training set. This shows that the molecule autoencoder can be combined with Bayesian optimization to discover new molecules with better properties than those found in the training set.

Bayesian optimization of chemical beauty Despite being difficult to quantify, drug-likeness is an important factor when selecting compounds during the early stages of the drug discovery process. Among other metrics, the Quantitative Estimation of Drug-likeness (QED) [36] can be used to quantify the degree to which key physicochemical properties of compounds agree with the ranges of values observed in approved drugs. Arguably, this measure captures the abstract notion of aesthetics in medicinal chemistry.

We used the molecule autoencoder to discover new drug-like molecules by optimizing the QED metric: we optimized eq. (1) with $\log P(m)$ replaced by $\text{QED}(m)$ after being normalized to have zero mean and unit standard deviation across the training data.

$$J^{\text{QED}}(m) = \text{QED}(m) - \text{SA}(m) - \text{ring-penalty}(m), \quad (2)$$

After 100 iterations of the data collection process, the best resulting molecule in terms of QED and not in the training data had $\text{QED} = 0.944$, which is only slightly worse than the best value found in the training set: $\text{QED} = 0.948$.

Panels c) and d) in Figure 4 show the top molecules obtained in this search; none of these were present in the training data. Panel c) shows the best ones according to the optimized aggregate score (1). Panel d) shows the best ones when considering only the QED metric. In the latter case, rather than large rings we observe molecules with antiaromatic rings (cyclobutadiene and cyclooctatetraene), which were filtered out when molecules were ranked according to the aggregate score (1). These moieties, although undesirable and non drug-like, are not penalized by the QED function. This underscores the importance of defining a complete objective function that combines all desired metrics.

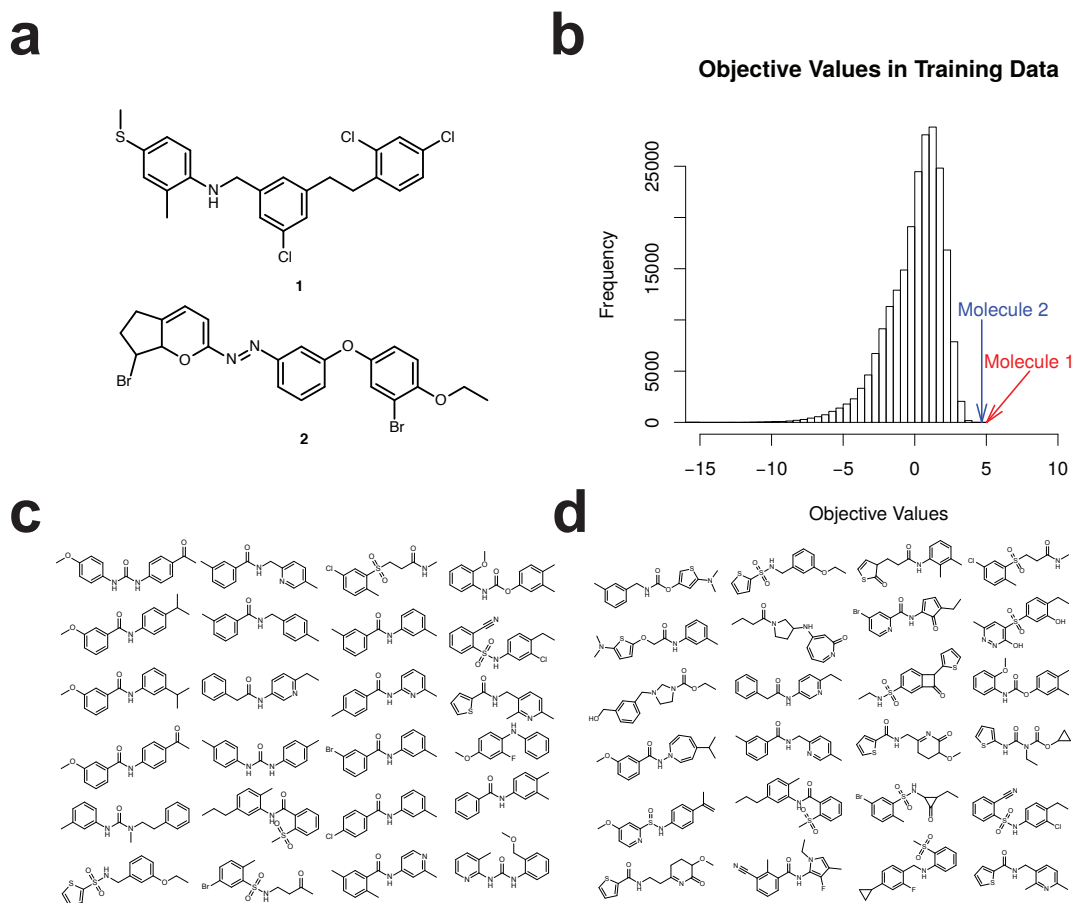


Figure 4: **a)** Molecules generated by the optimization process with better score values than any other molecule in the training data. **b)** Histogram of objective values in the training data. **c)** Optimization of The Quantitative Estimation of Drug-likeness. Top molecules with highest aggregate score 2 selected by the molecule autoencoder. QED values range from 0.915 to 0.812. **d)** Top molecules with highest J^{QED} selected by the molecule autoencoder. QED values range from 0.944 to 0.886.

Optimization of OLEDs Because of the large design space and promising properties of organic molecules as a replacement for solid-state inorganic materials, the field of organic electronics is very active in simulation-based molecular design, particularly in organic light emitting diodes (OLEDs).

OLEDs are organic molecules that emit light in response to an electric current. They are currently used in small displays, mostly smartphones, and have the potential to replace liquid-crystal displays with LED backpanels in larger displays. The newest OLED technology, thermally-assisted delayed fluorescence (TADF), [37] relies on combining fluorescent character of the emitter with a low energy difference between its lowest triplet and singlet excited state. Design proxies for these properties, together with characteristics such as emission color, are amenable to simple quantum calculations and recent works have addressed computer-driven design of new OLEDs both using TADF [9, 11, 38] and phosphorescence. [39] For this reason, we tested the performance of an autoencoder system on this class of molecules.

We used a training set with about 150,000 molecules generated by fragment combination. [9] Different properties of these molecules (emission color, delayed fluorescence decay rate (k_{TADF}), etc.) were originally estimated using time-dependent density functional theory. We then attempted to produce new molecules by optimizing these properties in the latent space.

We found that the latent vectors selected by the Bayesian optimization procedure did not usually translate into valid SMILES strings. The Bayesian optimization method attempts to collect data in regions of latent space far from the training data. Because the molecule autoencoder failed to learn a latent representation that generalizes to such distant regions, decoding optimized points led to invalid SMILES. This challenge to generalization is probably due to the fact that the OLED molecules are a grid-like combination of specific donor and acceptor moieties and thus lack diversity relative to the drug-like library. The lower accuracy reported in Table 1 for the OLED library is also a consequence of its combinatorial origins. These problems could potentially be addressed by training the molecule autoencoder using larger amounts of diverse, unlabeled molecules.

To avoid collecting data in those non-decodable regions, we attempted instead to perform a local optimization of three OLED molecules with good known experimental properties (F1, J1 and J2 [9]). In particular, we aimed at optimizing the delayed fluorescence decay rate, k_{TADF} , as predicted by a neural network trained to map from latent encodings to TADF. This network had 2 hidden layers and 50 units per layer. k_{TADF} is an excellent metric of TADF OLED performance, with the highest experimentally-known values being around $1 \mu\text{s}^{-1}$. Starting from an initial point in latent space, we performed a small number of steps by gradient ascent, decoding the latent vectors obtained at each iteration and then estimating their rate by quantum calculations.

Figure 5 shows the process of this local optimization. Molecule **3** is one of the three initial OLED molecules (J1), with $k_{\text{TADF}}^{\text{DFT}} = 0.004 \mu\text{s}^{-1}$. The rightmost molecule **6** shows the molecule obtained by decoding the latent point at the end of the optimization process (γ), with $k_{\text{TADF}}^{\text{DFT}} = 0.58 \mu\text{s}^{-1}$. The highest k_{TADF} in all training data is $0.9 \mu\text{s}^{-1}$. The molecules in-between (**4** and **5**) correspond to the decoding of intermediate latent points α and β . Interestingly, the analog of **5** where the complex ring is replaced by carbazole (a swapping of two adjacent characters in the SMILES) β has $k_{\text{TADF}}^{\text{DFT}} = 0.140 \mu\text{s}^{-1}$. Chemically, the changes in the structure concentrate on the electronic structure of the heteroaromatic system. Molecule **4** shows a carbazole unit that is slowly transformed to a phenoxazine group in

molecule **6**. Other changes include the position of the nitrogen atom in the pyridine groups as well as changing a benzene group to a pyridine.

These results indicate that the molecule autoencoder can be used for local compound optimization by gradient ascent. We were not able to obtain gains in k_{TADF} when starting from the other two initial OLED molecules (F1 and J2) because of inaccuracy in the neural network predictions for k_{TADF} .

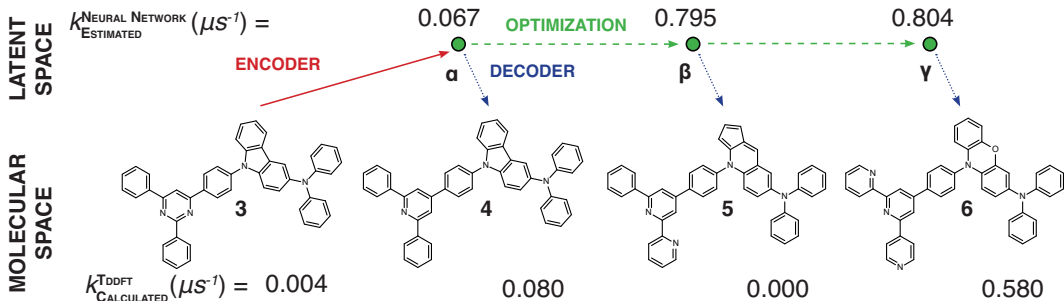


Figure 5: Starting from the molecule in the left, we follow in latent space the gradient of the predictions for k_{TADF} given by a neural network. We stop the optimization after a few steps, obtaining the molecule in the right, which has an improved k_{TADF} value. The molecules in-between represent intermediate optimization steps.

Discussion

We propose a new family of methods for exploring chemical space based on continuous encodings of molecules. These methods eliminate the need to hand-build libraries of compounds and allow a new type of directed gradient-based search through chemical space. We observed high fidelity and optimization ability when training with diverse representative data and less so with machine-generated combinatorial libraries. There are several avenues for further improvement of this approach to molecular design.

In this work, we used a text-based molecular encoding, but using a graph-based autoencoder would have several advantages. Forcing the decoder to produce valid SMILES strings makes the learning problem unnecessarily hard since the decoder must also implicitly learn which strings are valid SMILES. An autoencoder that directly outputs molecular graphs is appealing since it could explicitly address issues of graph isomorphism and the problem of strings that do not correspond to valid molecular graphs. Building an encoder which takes in molecular graphs is straightforward through the use of off-the-shelf molecular fingerprinting methods, such as ECFP [17] or a continuously-parameterized variant of ECFP such as neural molecular fingerprints. [18] However, building a neural network which can output arbitrary graphs is an open problem.

Both in the case of drug-like molecules and in OLED, the autoencoder sometimes produced molecules that are formally valid as graphs but contain moieties that are not desirable because of stability or synthetic constraints. Examples are acid chlorides, anhydrides, cyclopentadienes, aziridines, enamines, hemiaminals, enol ethers, cyclobutadiene,

and cycloheptatriene. Thus, the objective function to be optimized needs to capture as many desirable traits as possible and balance them to ensure that the optimizer focuses on genuinely desirable compounds.

In the current two-stage learning approach, the latent representation learned from unsupervised training might not smoothly map to the property being optimized. A straightforward way to address this problem would be to jointly train on both objectives. This would encourage the model to find a latent representation which is both easily decoded, and easy to predict with. [40]

The results reported in this work, and its application with carefully composed objective functions have the potential to create new avenues for molecular design.

Methods

Autoencoder architecture Strings of characters can be encoded into vectors using recurrent neural networks (RNNs). An encoder RNN can be paired with a decoder RNN to perform sequence-to-sequence learning. [41] We also experimented with convolutional networks for string encoding [42] and observed improved performance. This is explained by the presence of repetitive, translationally-invariant substrings that correspond to chemical substructures, e.g., cycles and functional groups.

Our SMILES-based text encoding used a subset 35 different characters. For ease of computation, we encoded strings up to a maximum length of 120 characters, although in principle there is no hard limit to string length. Shorter strings were padded with spaces to this same length. The structure of the VAE deep network was as follows: The encoder used three 1D convolutional layers of filter sizes 9, 9, 11 and 9, 9, 10 convolution kernels, respectively, followed by two fully-connected layers of width 435 and 292. The decoder started with a fully-connected layer of width 292, fed into three layers of gated recurrent unit (GRU) networks [43] with hidden dimension of 501.

We used the Keras [44] and Theano [45,46] packages to build and train this model.

The last layer of the RNN decoder defines a probability distribution over all possible characters at each position in the SMILES string. This means that the writeout operation is stochastic, and the same latent point may map to different SMILES strings, depending on the random seed used to sample characters. The output GRU layer had one additional input variable, corresponding to the character sampled from the softmax output of the previous neuron and was trained using teacher forcing. [47] This increased the accuracy of generated SMILES strings and resulted in higher fractions of valid SMILES strings for latent points outside the training data, but also made training more difficult, since the decoder showed a tendency to ignore the (variational) encoding and rely solely on the input sequence.

Bayesian optimization of molecules We trained a sparse Gaussian process (GP) model [48] with 500 inducing points to predict the cost of each molecule from the molecule’s feature vector. After this, we performed 10 iterations of Bayesian optimization using the expected improvement (EI) heuristic [49]. On each iteration, we selected a batch of 50 latent feature vectors by sequentially maximizing the EI acquisition function. To account for pending evaluations in the batch selection process we used the Kriging Believer Algorithm [50].

That is, after selecting each new data point in the batch, we added that data point as a new inducing point in the sparse GP model with associated target variable equal to the mean of the GP predictive distribution at that point. Once a new batch of 50 latent feature vectors was selected, each point in the batch was transformed into its corresponding SMILES string using the decoder network. From the SMILES string, we then obtained the corresponding score value using eqs. (1) and (2).

Acknowledgements

This work was supported financially by the Samsung Advanced Institute of Technology. The authors acknowledge the use of the Harvard FAS Odyssey Cluster and support from FAS Research Computing.

JMHL acknowledges support from the Rafael del Pino Foundation. RPA acknowledges support from the Alfred P. Sloan Foundation and NSF IIS-1421780. AAG acknowledges support from The Department of Energy, Office of Basic Energy Sciences under award DE-SC0015959.

Author contributions

DD conceived the project; RGB and DD designed the approach; RGB trained the autoencoder and performed latent space encode-decode experiments with assistance from TH and JAG; JMHL designed and performed the Bayesian optimization of logP, QED and k_{TADF} metrics and the local optimization of OLED molecule; RPA and AAG supervised the project; RGB, DD and JMHL wrote the first version of the manuscript. All authors contributed to the design of the methodology and experimental setup, the analysis of the results and the writing of the manuscript.

Competing financial interests

The authors declare no competing financial interests.

Availability of computer code

A open-source version of the computer code used to create the VAE in this work is available at <https://github.com/HIPS/molecule-autoencoder>. Third-party implementations are also available.

References

- [1] Kim, S. *et al.* PubChem Substance and Compound databases. *Nucleic Acids Res.* **44**, D1202–D1213 (2016).
- [2] Polishchuk, P. G., Madzhidov, T. I. & Varnek, A. Estimation of the size of drug-like chemical space based on GDB-17 data. *J. Comput.-Aided Mol. Des.* **27**, 675–679 (2013).

- [3] Shoichet, B. K. Virtual screening of chemical libraries. *Nature* **432**, 862–5 (2004).
- [4] Scior, T. *et al.* Recognizing Pitfalls in Virtual Screening: A Critical Review. *J. Chem. Inf. Model.* **52**, 867–881 (2012).
- [5] Cheng, T., Li, Q., Zhou, Z., Wang, Y. & Bryant, S. H. Structure-Based Virtual Screening for Drug Discovery: a Problem-Centric Review. *AAPS J.* **14**, 133–141 (2012).
- [6] Pyzer-Knapp, E. O., Suh, C., Gómez-Bombarelli, R., Aguilera-Iparraguirre, J. & Aspuru-Guzik, A. What is high-throughput virtual screening? a perspective from organic materials discovery. *Annu. Rev. Mater. Res.* **45**, 195–216 (2015). URL <http://dx.doi.org/10.1146/annurev-matsci-070214-020823>. <http://dx.doi.org/10.1146/annurev-matsci-070214-020823>.
- [7] Schneider, G. Virtual screening: an endless staircase? *Nat. Rev. Drug Discov.* **9**, 273–276 (2010). URL <http://dx.doi.org/10.1038/nrd3139>.
- [8] Hachmann, J. *et al.* The Harvard clean energy project: large-scale computational screening and design of organic photovoltaics on the world community grid. *J. Phys. Chem. Lett.* **2**, 2241–2251 (2011).
- [9] Gómez-Bombarelli, R. *et al.* Design of efficient molecular organic light-emitting diodes by a high-throughput virtual screening and experimental approach **15**, 1120–1127.
- [10] Virshup, A. M., Contreras-García, J., Wipf, P., Yang, W. & Beratan, D. N. Stochastic Voyages into Uncharted Chemical Space Produce a Representative Library of All Possible Drug-Like Compounds. *J. Am. Chem. Soc.* **135**, 7296–7303 (2013). URL <http://dx.doi.org/10.1021/ja401184g>.
- [11] Rupakheti, C., Virshup, A., Yang, W. & Beratan, D. N. Strategy To Discover Diverse Optimal Molecules in the Small Molecule Universe. *J. Chem. Inf. Model.* **55**, 529–537 (2015). URL <http://dx.doi.org/10.1021/ci500749q>.
- [12] Reymond, J.-L. The Chemical Space Project. *Acc. Chem. Res.* **48**, 722–730 (2015). URL <http://dx.doi.org/10.1021/ar500432k>.
- [13] Reymond, J.-L., van Deursen, R., Blum, L. C. & Ruddigkeit, L. Chemical space as a source for new drugs. *Med. Chem. Commun.* **1**, 30 (2010). URL <http://dx.doi.org/10.1039/c0md00020e>.
- [14] Kanal, I. Y., Owens, S. G., Bechtel, J. S. & Hutchison, G. R. Efficient computational screening of organic polymer photovoltaics. *J. Phys. Chem. Lett.* **4**, 1613–1623 (2013). URL <http://dx.doi.org/10.1021/jz400215j>. PMID: 26282968, <http://dx.doi.org/10.1021/jz400215j>.
- [15] OBoyle, N. M., Campbell, C. M. & Hutchison, G. R. Computational design and selection of optimal organic photovoltaic materials. *J. Phys. Chem. C* **115**, 16200–16210 (2011). URL <http://dx.doi.org/10.1021/jp202765c>. <http://dx.doi.org/10.1021/jp202765c>.

- [16] van Deursen, R. & Reymond, J.-L. Chemical Space Travel. *ChemMedChem* **2**, 636–640 (2007). URL <http://dx.doi.org/10.1002/cmdc.200700021>.
- [17] Rogers, D. & Hahn, M. Extended-Connectivity Fingerprints. *J. Chem. Inf. Model.* **50**, 742–754 (2010).
- [18] Duvenaud, D. K. *et al.* Convolutional Networks on Graphs for Learning Molecular Fingerprints. In *Advances in Neural Information Processing Systems*, 2215–2223 (2015).
- [19] Kearnes, S., McCloskey, K., Berndl, M., Pande, V. & Riley, P. Molecular Graph Convolutions: Moving Beyond Fingerprints. *ArXiv e-prints* (2016). 1603.00856.
- [20] Hansen, K. *et al.* Machine learning predictions of molecular properties: Accurate many-body potentials and nonlocality in chemical space. *The Journal of Physical Chemistry Letters* **6**, 2326–2331 (2015). URL <http://dx.doi.org/10.1021/acs.jpclett.5b00831>. PMID: 26113956, <http://dx.doi.org/10.1021/acs.jpclett.5b00831>.
- [21] Rupp, M., Tkatchenko, A., Mller, K.-R. & von Lilienfeld, O. A. Fast and Accurate Modeling of Molecular Atomization Energies with Machine Learning. *Phys. Rev. Lett.* **108** (2012). URL <http://dx.doi.org/10.1103/physrevlett.108.058301>.
- [22] Hirn, M., Poilvert, N. & Mallat, S. Quantum Energy Regression using Scattering Transforms. *ArXiv e-prints* (2015). 1502.02077.
- [23] Schütt, K. T., Arbabzadah, F., Chmiela, S., Müller, K. R. & Tkatchenko, A. Quantum-Chemical Insights from Deep Tensor Neural Networks. *ArXiv e-prints* (2016). 1609.08259.
- [24] Radford, A., Metz, L. & Chintala, S. Unsupervised Representation Learning with Deep Convolutional Generative Adversarial Networks. *arXiv preprint arXiv:1511.06434* (2015).
- [25] Bowman, S. R. *et al.* Generating Sentences from a Continuous Space. *arXiv preprint arXiv:1511.06349* (2015).
- [26] van den Oord, A. *et al.* WaveNet: A Generative Model for Raw Audio. *ArXiv e-prints* (2016). 1609.03499.
- [27] Weininger, D. SMILES a chemical language and information system. 1. Introduction to methodology and encoding rules. *J. Chem. Inf. Model.* **28**, 31–36 (1988). URL <http://dx.doi.org/10.1021/ci00057a005>.
- [28] Heller, S., McNaught, A., Stein, S., Tchekhovskoi, D. & Pletnev, I. Inchi - the worldwide chemical structure identifier standard. *J. Cheminf.* **5**, 7 (2013).
- [29] RDKit: Open-source cheminformatics. <http://www.rdkit.org>. [Online; accessed 11-April-2013].
- [30] Kingma, D. P. & Welling, M. Auto-encoding variational bayes. *arXiv preprint arXiv:1312.6114* (2013).

- [31] Irwin, J. J., Sterling, T., Mysinger, M. M., Bolstad, E. S. & Coleman, R. G. Zinc: A free tool to discover chemistry for biology. *J. Chem. Inf. Model.* **52**, 1757–1768 (2012). URL <http://dx.doi.org/10.1021/ci3001277>. PMID: 22587354, <http://dx.doi.org/10.1021/ci3001277>.
- [32] Snoek, J., Larochelle, H. & Adams, R. P. Practical Bayesian Optimization of Machine Learning Algorithms. In *Neural Information Processing Systems 25* (2012).
- [33] Law, V. *et al.* Drugbank 4.0: shedding new light on drug metabolism. *Nucleic Acids Res.* **42**, D1091–D1097 (2014). URL <http://nar.oxfordjournals.org/content/42/D1/D1091.abstract>. <http://nar.oxfordjournals.org/content/42/D1/D1091.full.pdf+html>.
- [34] Ertl, P. & Schuffenhauer, A. Estimation of synthetic accessibility score of drug-like molecules based on molecular complexity and fragment contributions. *J. Cheminf.* **1**, 1–11 (2009). URL <http://dx.doi.org/10.1186/1758-2946-1-8>.
- [35] Wildman, S. A. & Crippen, G. M. Prediction of physicochemical parameters by atomic contributions. *J. Chem. Inf. Comput. Sci.* **39**, 868–873 (1999). URL <http://dx.doi.org/10.1021/ci9903071>. <http://dx.doi.org/10.1021/ci9903071>.
- [36] Bickerton, G. R., Paolini, G. V., Besnard, J., Muresan, S. & Hopkins, A. L. Quantifying the chemical beauty of drugs. *Nature chemistry* **4**, 90–98 (2012).
- [37] Uoyama, H., Goushi, K., Shizu, K., Nomura, H. & Adachi, C. Highly efficient organic light-emitting diodes from delayed fluorescence. *Nature* **492**, 234–238 (2012). URL <http://dx.doi.org/10.1038/nature11687>.
- [38] Shu, Y. & Levine, B. G. Simulated evolution of fluorophores for light emitting diodes. *J. Chem. Phys.* **142** (2015). URL <http://scitation.aip.org/content/aip/journal/jcp/142/10/10.1063/1.4914294>.
- [39] Kwak, H. S. *et al.* Virtual screening and evaluation of highly efficient organometallic light-emitting materials (2016). URL <http://dx.doi.org/10.1117/12.2237951>.
- [40] Snoek, J., Adams, R. P. & Larochelle, H. Nonparametric guidance of autoencoder representations using label information. *Journal of Machine Learning Research* **13**, 2567–2588 (2012).
- [41] Sutskever, I., Vinyals, O. & Le, Q. V. Sequence to sequence learning with neural networks. In *Advances in neural information processing systems*, 3104–3112 (2014).
- [42] Kalchbrenner, N., Grefenstette, E. & Blunsom, P. A Convolutional Neural Network for Modelling Sentences. *Proceedings of the 52nd Annual Meeting of the Association for Computational Linguistics* (2014).
- [43] Chung, J., Gülçehre, Ç., Cho, K. & Bengio, Y. Empirical evaluation of gated recurrent neural networks on sequence modeling. *CoRR* **abs/1412.3555** (2014). URL <http://arxiv.org/abs/1412.3555>.

- [44] Chollet, F. keras. <https://github.com/fchollet/keras> (2015).
- [45] Bastien, F. *et al.* Theano: new features and speed improvements. Deep Learning and Unsupervised Feature Learning NIPS 2012 Workshop (2012).
- [46] Theano Development Team. Theano: A Python framework for fast computation of mathematical expressions. *arXiv e-prints* **abs/1605.02688** (2016). URL <http://arxiv.org/abs/1605.02688>.
- [47] Williams, R. J. & Zipser, D. A learning algorithm for continually running fully recurrent neural networks. *Neural Comput.* **1**, 270–280 (1989). URL <http://dx.doi.org/10.1162/neco.1989.1.2.270>.
- [48] Snelson, E. & Ghahramani, Z. Sparse Gaussian processes using pseudo-inputs. In *Advances in neural information processing systems*, 1257–1264 (2005).
- [49] Jones, D. R., Schonlau, M. & Welch, W. J. Efficient global optimization of expensive black-box functions. *J. Global Optim.* **13**, 455–492 (1998).
- [50] Cressie, N. The origins of kriging. *Math. Geol.* **22**, 239–252 (1990). URL <http://dx.doi.org/10.1007/bf00889887>.

Supplementary Material

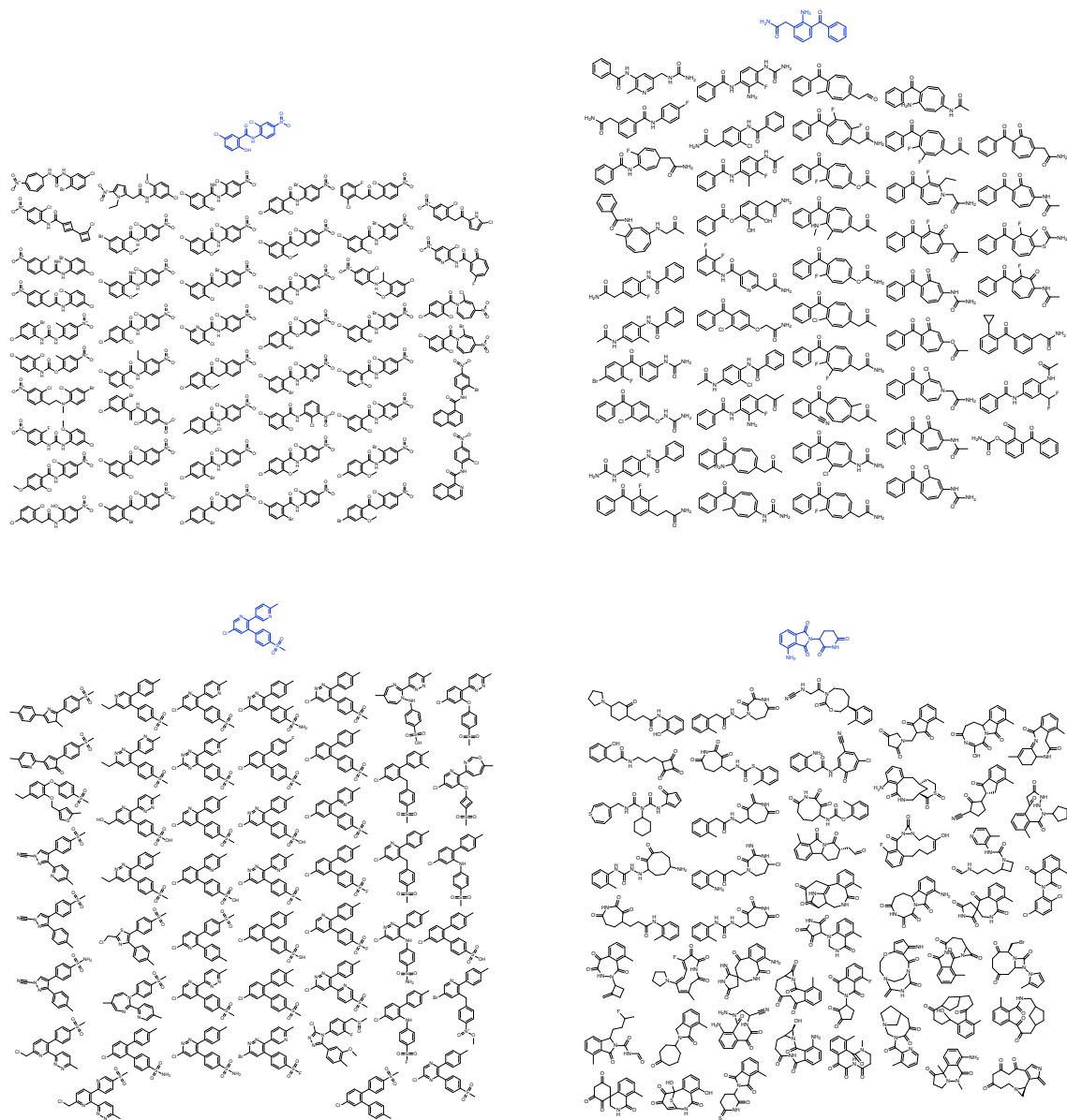


Figure 6: Molecules which were used as inputs to the variational autoencoder, presented with decodings of multiple samples from the encoding distribution

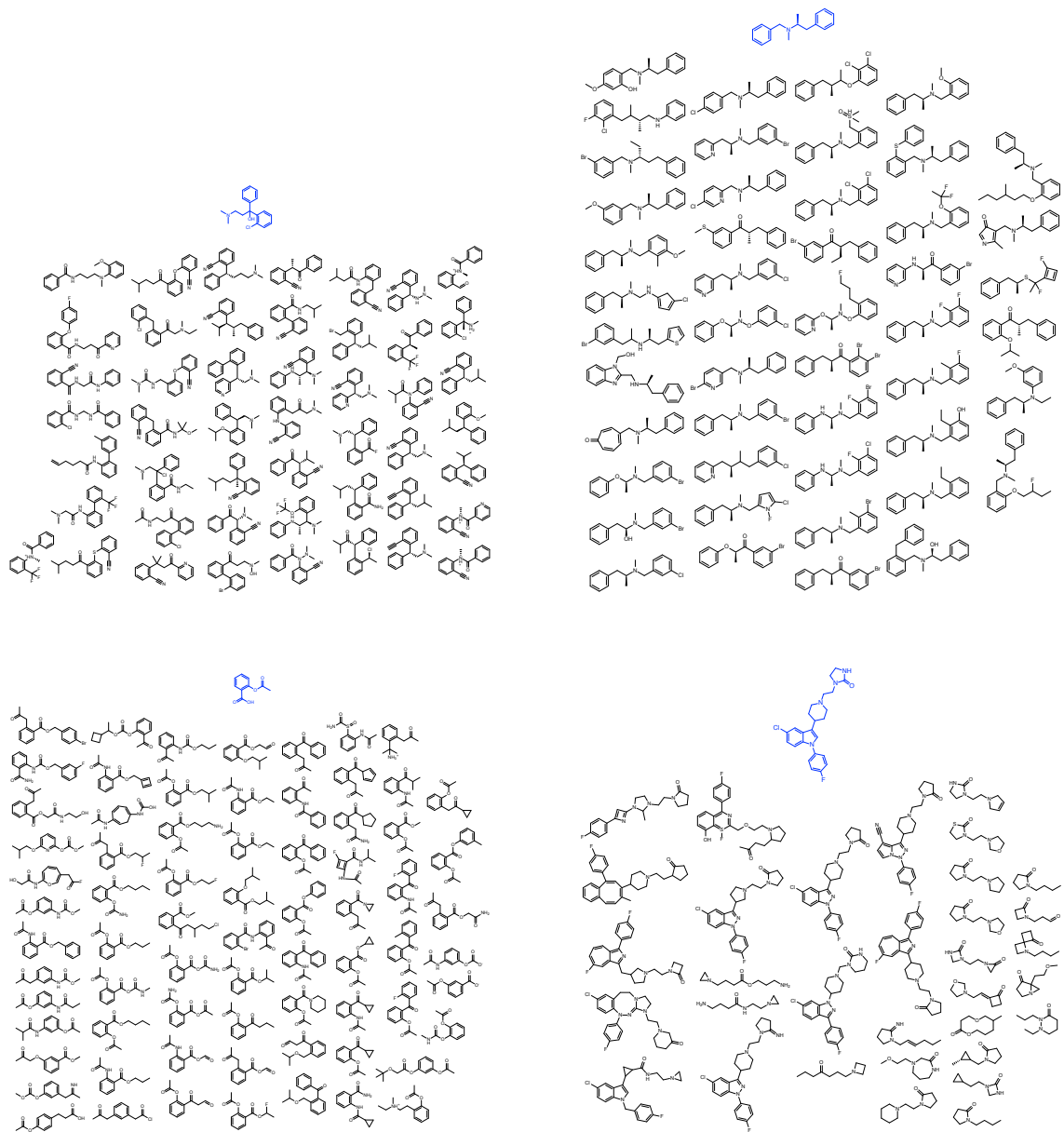


Figure 7: In blue, molecules which were used as inputs to the variational autoencoder, presented with decodings of multiple samples from the encoding distribution.

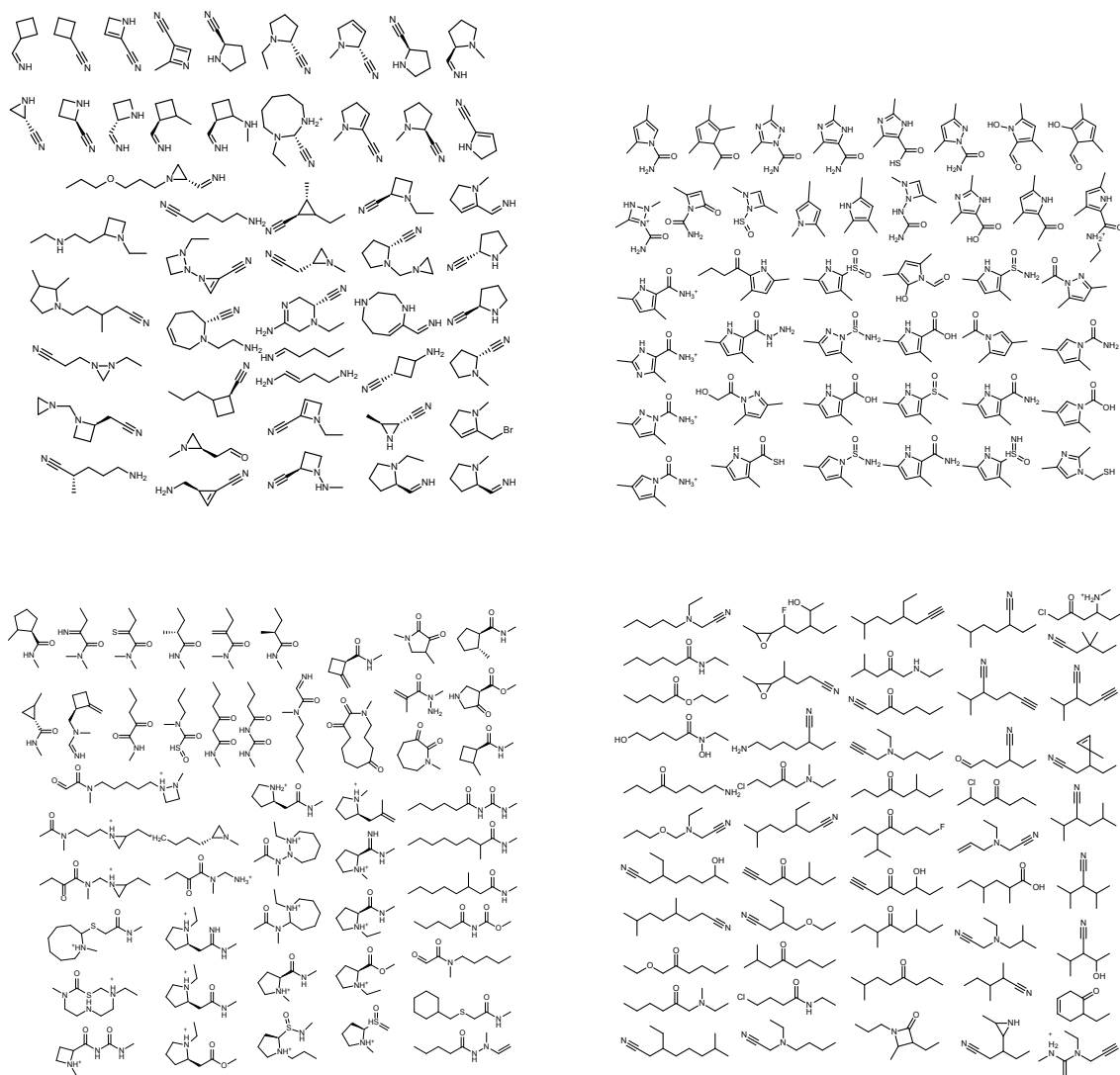


Figure 8: Molecules decoded from randomly-sampled points in the latent space of a variational autoencoder.

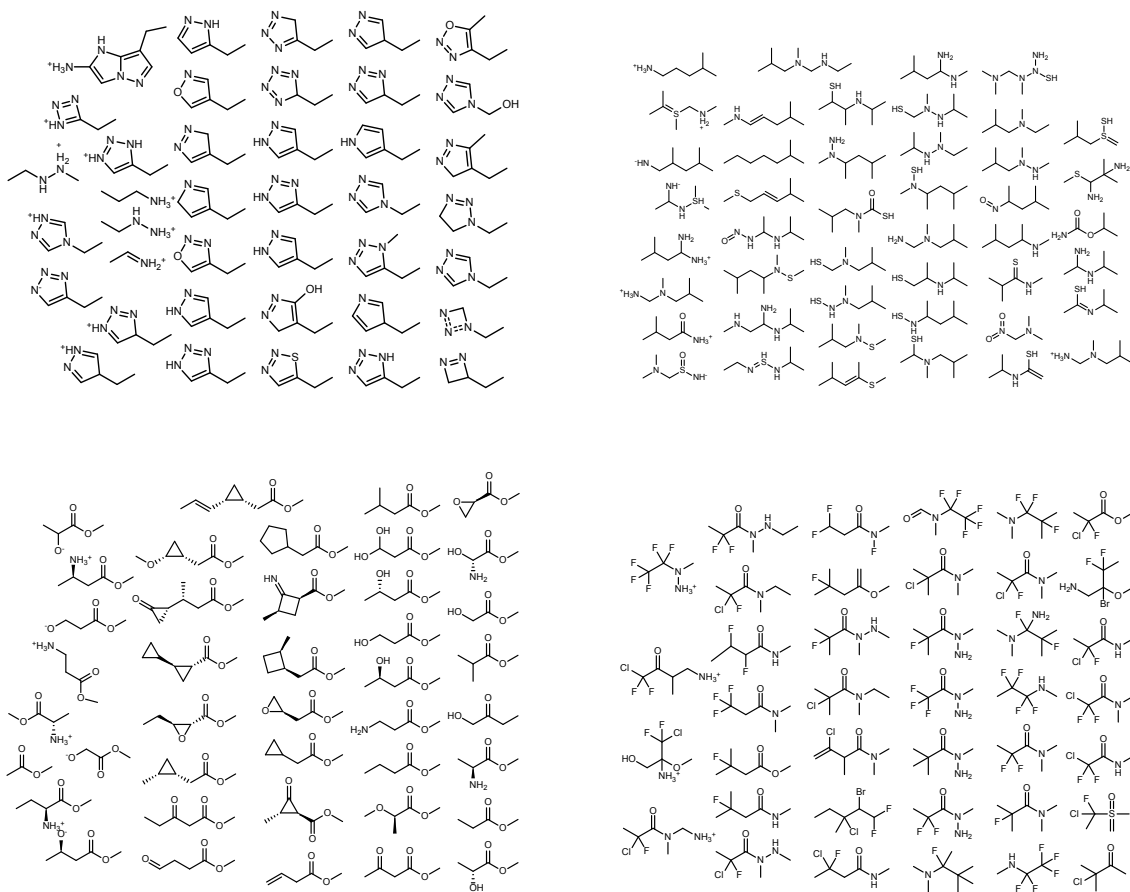


Figure 9: Molecules decoded from randomly-sampled points in the latent space of a variational autoencoder.

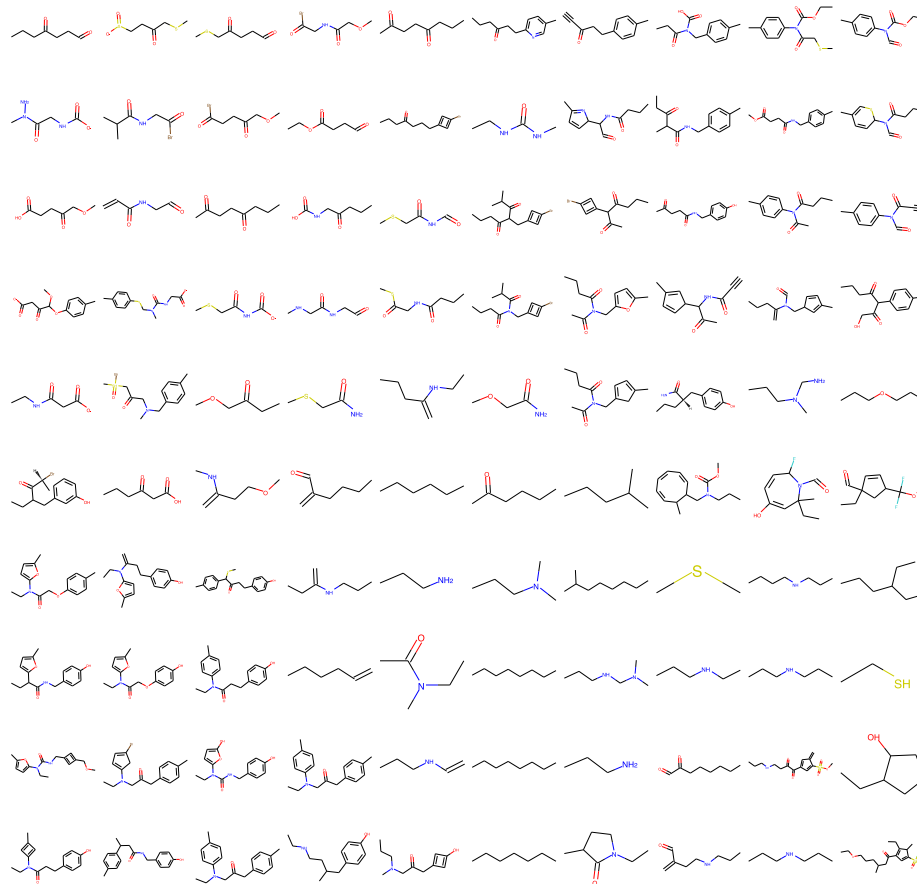


Figure 10: Two-dimensional interpolation between four random points in in drug-like VAE. Decodings of interpolating linearly between the latent representations of the four molecules in the corners.

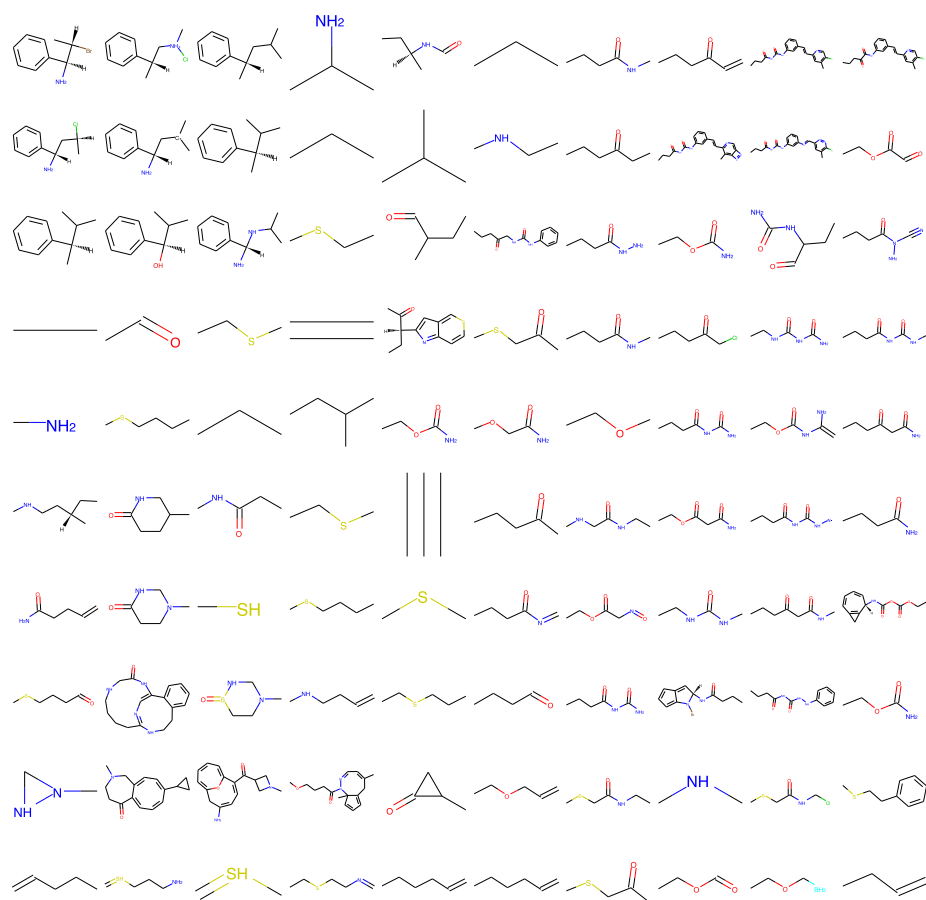


Figure 11: Two-dimensional interpolation between four random points in in drug-like VAE. Decodings of interpolating linearly between the latent representations of the four molecules in the corners.

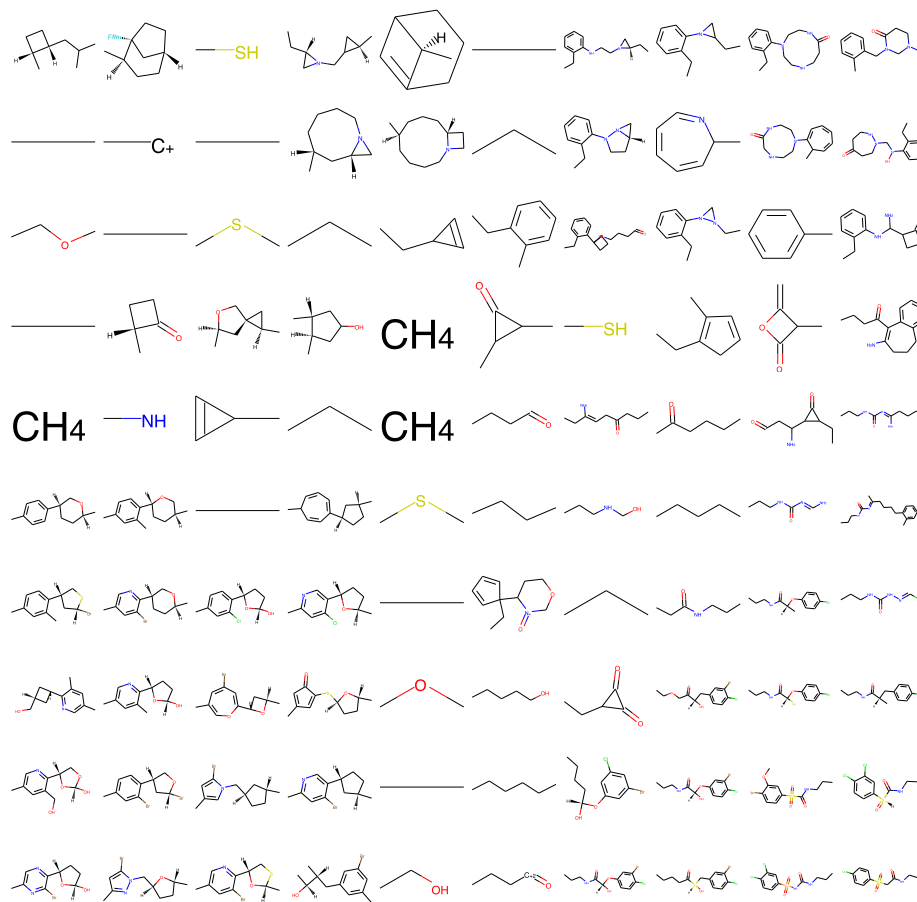


Figure 12: Two-dimensional interpolation between four random points in in drug-like VAE. Decodings of interpolating linearly between the latent representations of the four molecules in the corners.

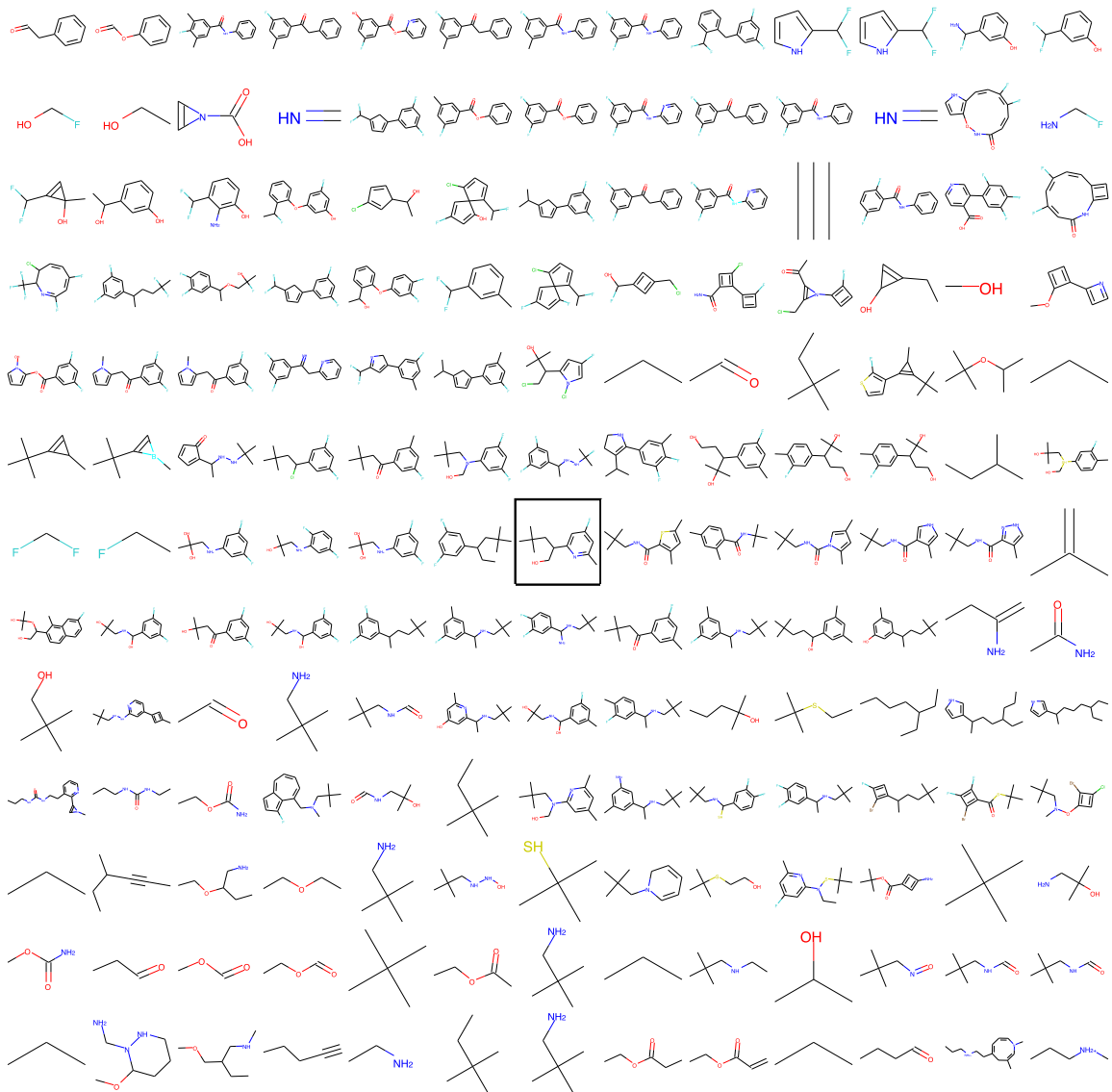


Figure 13: Starting from the molecule in the center, two random, unit-length vectors were followed in latent space for increasingly large displacements. This defines a random two-dimensional plane in the 56-dimensional latent space. At each location in this two-dimensional subspace, we show the molecule most likely to be decoded at that point in the latent space. Nearby points decode to similar molecules, and distant points decode to a wide variety of compounds.

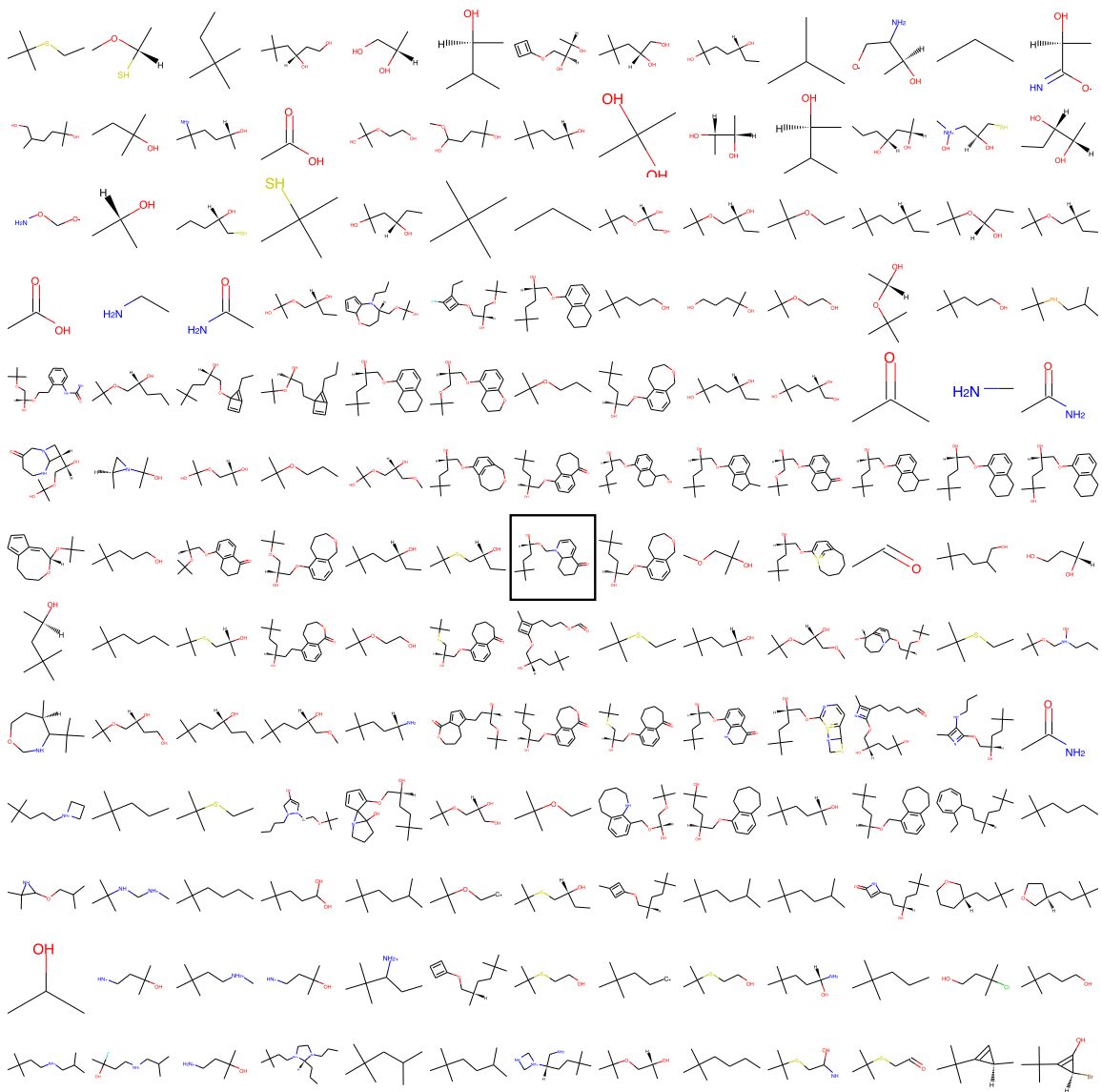


Figure 14: Starting from the molecule in the center, two random, unit-length vectors were followed in latent space for increasingly large displacements.

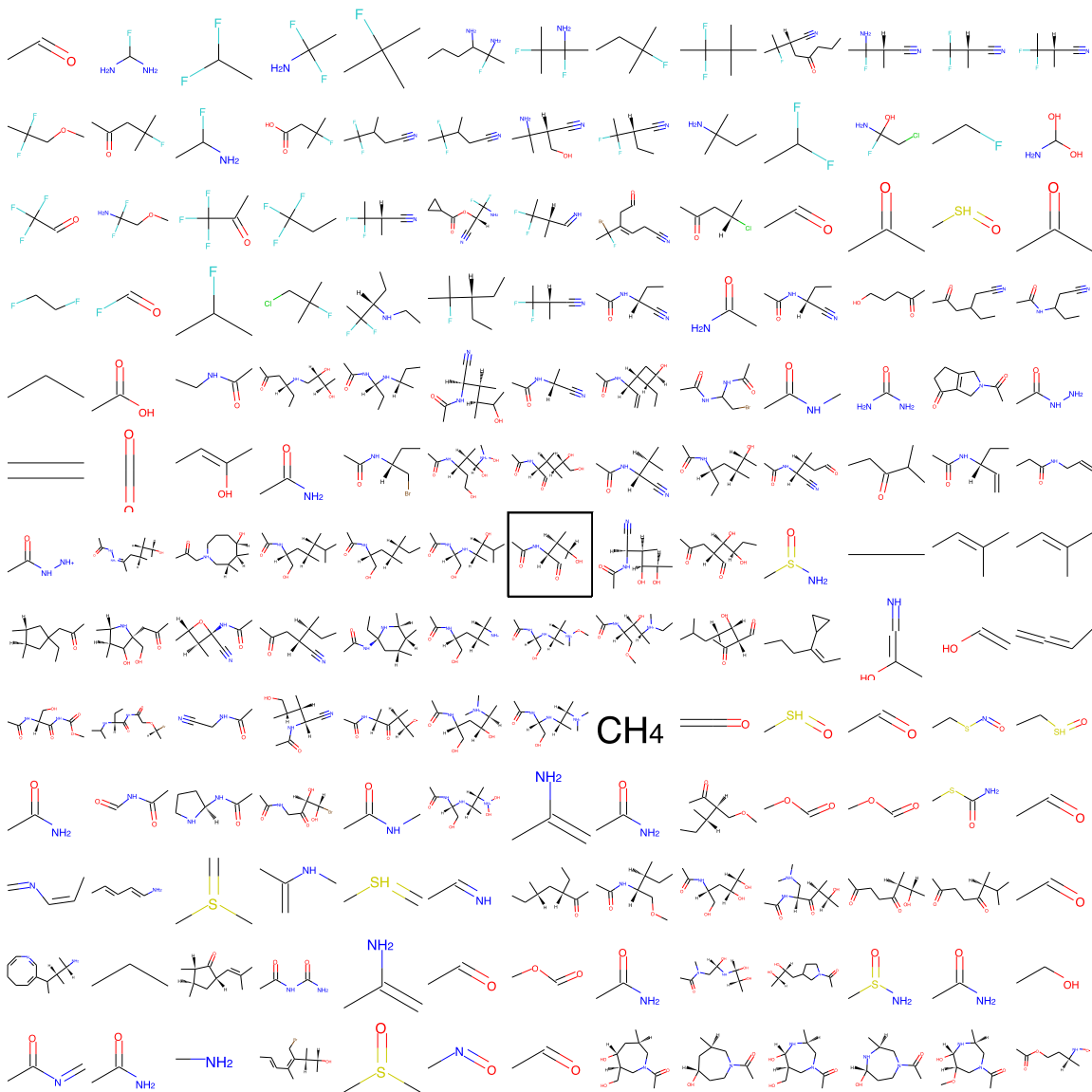


Figure 15: Starting from the molecule in the center, two random, unit-length vectors were followed in latent space for increasingly large displacements.